UC Davis
UC Davis Previously Published Works

Title
Assignment of oriented sample NMR resonances from a three transmembrane helix protein

Permalink
https://escholarship.org/uc/item/5c2358mq

Authors
Murray, DT
Hung, I
Cross, TA

Publication Date
2014-03-01

DOI
10.1016/j.jmr.2013.12.014

Peer reviewed

eScholarship.org Powered by the California Digital Library
University of California

NIH Public Access
Author Manuscript
J Magn Reson. Author manuscript; available in PMC 2015 March 01.

Published in final edited form as:
J Magn Reson. 2014 March ; 240: 34–44. doi:10.1016/j.jmr.2013.12.014.

Assignment of Oriented Sample NMR Resonances from a Three Transmembrane Helix Protein

D. T. Murray[a,b], **I. Hung**[b], and **T. A. Cross**[a,b,c,*]

[a]Institute for Molecular Biophysics, Florida State University, Tallahassee, FL, 32306, USA

[b]National High Magnetic Field Laboratory, Tallahassee, FL, 32310, USA

[c]Department of Chemistry and Biochemistry, Florida State University, Tallahassee, FL, 32306, USA

Abstract

Oriented sample solid state NMR techniques have been routinely employed to determine the structures of membrane proteins with one or two transmembrane helices. For larger proteins the technique has been limited by spectral resolution and lack of assignment strategies. Here, a strategy for resonance assignment is devised and applied to a three transmembrane helix protein. Sequence specific assignments for all labeled transmembrane amino acid sites are obtained, which provide a set of orientational restraints and helix orientation in the bilayer. Our experiments expand the utility of solid state NMR in membrane protein structure characterization to three transmembrane helix proteins and represent a straightforward strategy for routinely characterizing multiple transmembrane helix protein structures.

Keywords

membrane protein; lipid bilayer; oriented sample solid state NMR; resonance assignment; helix orientation; Mycobacterium tuberculosis; membrane protein structure

1. Introduction

The majority of membrane protein structures determined by solid state NMR (ssNMR) and deposited in the Protein Data Bank rely on orientational restraints obtained from oriented sample (OS) methods. Routine application of OS ssNMR to proteins with more than one or two transmembrane (TM) helices has yet to be achieved. The primary obstacles for characterizing larger proteins are spectral resolution and resonance assignment strategies. Due to the importance of membrane proteins in disease and the paucity of structures of this class in the PDB, it is important to expand the OS ssNMR technique to encompass larger proteins.

Protein structure is dictated by the sum of the intra-protein interactions and the protein's interactions with its environment [1]. It is becoming increasingly clear that the use of environments other than lipid bilayers as a model for membrane protein structures can lead

© 2014 Elsevier Inc. All rights reserved.

*Corresponding author: cross@magnet.fsu.edu, 1800 Paul Dirac Drive, Tallahasssee, FL, 32310, (850) 644-0917.

Publisher's Disclaimer: This is a PDF file of an unedited manuscript that has been accepted for publication. As a service to our customers we are providing this early version of the manuscript. The manuscript will undergo copyediting, typesetting, and review of the resulting proof before it is published in its final citable form. Please note that during the production process errors may be discovered which could affect the content, and all legal disclaimers that apply to the journal pertain.

NIH-PA Author Manuscript
NIH-PA Author Manuscript
NIH-PA Author Manuscript

NIH-PA Author Manuscript

NIH-PA Author Manuscript

NIH-PA Author Manuscript

to severe structural distortions [2–7]. Therefore, it is imperative to determine structures in the most native-like environment possible, such as lipid bilayers. X-ray crystallography is mainly responsible for the current structures of membrane proteins with more than three TM helices or those that form large oligomeric structures [8, 9]. These structures are determined in a detergent stabilized crystalline environment that poorly mimics the bilayer thickness, the dielectric and water concentration gradients, and the pressure profile of native membranes [10, 11]. One reason for the lack of success with smaller proteins is the scarcity of strong interhelical interactions [10, 11] that would stabilize tertiary and or quaternary protein structure in a crystal lattice. Solution state NMR has made some progress with small helical membrane proteins [12, 13], but concerns have been voiced regarding the structural distortions observed in solution NMR structures for membrane proteins solubilized in detergent micelles [5, 14]. This is mainly because the detergent micelle has a weak hydrophobic environment, water accessibility into the micelle interior, a poorly defined hydrophobic thickness, and a single highly curved hydrophilic surface. Electron crystallography has been used to determine atomic resolution structures for proteins in 2D crystals containing lipid [15, 16]. However, the relatively few lipid molecules in these preparations may not adequately mimic the native membrane properties. Electron tomography also has the ability to characterize protein structure in lipid bilayers [8, 17] but only with low resolution (currently ~3–7 Å). To date, ssNMR spectroscopy is the only technique capable of characterizing membrane protein structure at atomic resolution in lipid bilayers [18–24]. Due to the importance of the lipid bilayer for achieving native structures it is necessary to further develop solid state NMR technology and methodology for routine characterization of small, helical membrane protein structures.

While a majority of spectroscopic effort in ssNMR is currently being dedicated to MAS techniques, most of the structures that have been characterized utilize orientational structural restraints [25, 26], primarily obtained from OS ssNMR experiments. Recently, MAS experiments on rotationally aligned proteins in liposomes have been used to obtain similar restraints [20, 21, 27]. Together, these methods show ssNMR is capable of characterizing the structure for proteins with up to seven TM helices [18–24, 28]. Either way, orientational restraints provide precise restraints for the backbone peptide planes relative to the membrane normal [29–31]. Additionally, an advantage of OS ssNMR is that helix tilt and rotation angles can be determined for uniform sections of helical structures. In other words, the structure achieved with these restraints is oriented relative to the lipid bilayer, a feature that is unique to ssNMR. It should be noted that for multiple TM helix proteins, tertiary structural restraints, such as interhelical distances are also needed. Fortunately, only a sparse number of distance restraints are required to calculate a tertiary structure when combined with orientational restraints [25]. These distances can be obtained from MAS ssNMR [14, 19, 25]. Together, OS and MAS ssNMR techniques represent a versatile toolbox for the determination of membrane protein structure.

Sequence specific assignments have been a challenge for OS ssNMR Separated Local Field (SLF) spectra of membrane proteins in aligned lipid bilayers. For proteins with one or two helices, amino acid (AA) specific ^{15}N-labeled samples are sufficient to fix helix tilt and rotation angles. Given a well resolved spectrum [18–24], resonance assignments can be directly obtained. Computational approaches have been developed to assign resonances based on such spectra and also obtain estimates of helix tilt and rotation angles [31–33]. Recently, clever methods have been developed to spectroscopically assign the resonances in SLF spectra of uniformly labeled samples by correlating anisotropic ^{15}N chemical shifts of *i* and *i*+1 residues [34, 35]. While these methods have been useful for assigning the resonances in high sensitivity, single TM helix peptides, the lower sensitivity of multiple helix proteins makes 3D experiments prohibitive; given the low intensity of crosspeaks (~15% of the diagonal) [35] that require significant signal averaging leading to long

NIH-PA Author Manuscript

NIH-PA Author Manuscript

NIH-PA Author Manuscript

experimental times. Furthermore, the increased spectral overlap for these proteins makes encoding the *i*, *i*+1 correlations in a 2D experiment [34] difficult, thereby defeating the resonance assignment strategy. It is useful then to try to interpret SLF spectra for larger membrane proteins without these experiments.

To illustrate the potential of OS ssNMR to assist in a tertiary structure calculation, we have chosen to study the membrane protein Rv1861 from *Mycobacterium tuberculosis* (*Mtb*). Tuberculosis is responsible for 1.4 million deaths per year and currently there exist extensively drug resistant strains. Many small membrane proteins in the cell envelope are priority drug targets for structural characterization. Rv1861 is a small helical membrane protein involved in transglycosylase activity [36]. It is predicted to contain three TM helices in a short 101 amino acid sequence which minimizes the loop and termini lengths, providing a simple system to investigate the TM domain without interference from a large extramembranous domain. Initial OS ssNMR spectra for the protein in mechanically aligned lipid bilayers have been published [37].

Here, a strategy is demonstrated for assigning the resonances of TM sites in SLF spectra of Rv1861 in a synthetic lipid bilayer. Due to a high level of congestion in OS ssNMR data for uniformly labeled protein, a series of AA specific ^{15}N-labeled samples were prepared covering seven of the hydrophobic amino acid types in the TM domain. The AA specific ^{15}N-labeled samples allowed resolution of almost all of the TM helix sites in all three helices of Rv1861. The devised assignment strategy is suitable for interpreting spectra from membrane proteins with three and potentially more TM helices. This strategy is based on the unique amino acid distribution in the TM helices and dictates which amino acid types should be labeled and in what order. Resonances are assigned first by focusing on a select few residues in the middle of the helices where the structure is expected to be more uniform and then extrapolating the assignments toward the potentially less ordered termini of the helices. Finally, the sequence specific assignments achieved here provide a set of high resolution orientational restraints that can be readily used in a tertiary structure calculation.

2. Materials and Methods

2.1 Protein expression, Purification and Reconstitution

Protein was expressed as previously described [38] with an N-terminal His_6 tag for purification. Three 1 L cultures were grown in luria broth (LB) media with shaking at 37 °C to an OD_{600} value of 1.5 (1 cm pathlength). The cells were harvested, combined and resuspended in 30 mL of sterile M9 salts to wash away residual LB media from the cells. The cells were pelleted again and then resuspended in 1 L of M9 salts supplemented with 4 g/L D-glucose, 100 mg of a ^{15}N-labeled L-amino acid (Cambridge Isotope Labs, Inc. or Sigma-Aldrich, Inc.) and an unlabeled amino acid mix covering all remaining amino acids (Supplemental Table 1). Cultures were grown for an additional 30 min and then induced by adding IPTG to a final concentration of 0.4 mM. After an additional 1 h of growth the cells were harvested and then resuspended in 10 mL of lysis buffer (40 mM HEPES pH 7.5, 500 mM sodium chloride) per unit of OD_{600} absorbance for the culture and frozen at −80 °C for at least 24 h.

Cells were thawed at room temperature and 0.25 mg/mL of lysozyme (EMD, Inc.) was added along with 4 μL Benzonase (Novagen, Inc.) before incubating on an orbital shaker at room temperature for 30 min. Cells were lysed by french press (Thermo Scientific, Inc.) at 12,000 PSI three times. Inclusion body fractions containing the Rv1861 protein were isolated by centrifugation at 18,000 g for 1 h at 12 °C. The pellets were resuspended in solubilization buffer (40 mM HEPES pH 7.5, 300 mM sodium chloride, 3% v/v Empigen-BB) to the same volume used to store the cell pellets. The mixture was incubated at 4 °C

NIH-PA Author Manuscript

NIH-PA Author Manuscript

NIH-PA Author Manuscript

with rotation for 8–12 h. Prior to purification the mixture was centrifuged at 228,000 g for 30 min to remove any insoluble material. The mixture was loaded onto a 5 mL HIS-PrepFF Nickel Affinity column (GE Lifesciences, Inc) equilibrated with equilibration buffer (40 mM HEPES pH 7.5, 300 mM sodium chloride, 0.7% v/v Empigen-BB) using an AKTA Xpress (GE Lifesciences, Inc.) purification system. The column was washed with wash buffer (equilibration buffer with 40 mM imidazole) until the UV absorbance returned to baseline. The wash buffer was replaced with four column volumes of exchange buffer (1.5% w/v decyl-dimethylglycine (DDGly), 20 mM HEPES pH 7.5) before eluting the protein in the elute buffer (exchange buffer with 500 mM imidazole). Typically 15–30 mg of protein in 10 mL buffer was obtained per 1 L of M9 media.

Dimyristolphosphatidylcholine/dimyristolphosphatidylglycerol (DMPC/DMPG) liposomes were prepared by dissolving 50 mg of lipid powder (Avanti Polar Lipids, Inc.) at a 4:1 molar ratio in 2 mL of 10 mM HEPES pH 7.5. The mixture was bath sonicated (Branson, Inc) in a glass test tube until clear before adding a 20% w/v solution of DDGly to a concentration of 2.5% w/v. After mixing the lipids and detergent, a volume (~3 mL) equivalent to 10.5 mg of protein was added. The volume was then adjusted to 8 mL with 10 mM HEPES pH 7.5. The solution was gently mixed and incubated at 37 °C overnight. The sample was then dialyzed against 2 L of 10 mM HEPES pH 7.5 at 35 °C (6–8 kDa cutoff dialysis tubing, SpectraPor, Inc.) for three days with twice daily buffer changes to remove detergent. Proteoliposomes were harvested by centrifugation at 228,000 g for 1.5 h and resuspended in 1.2 mL of 10 mM HEPES pH 7.5, 0.01% w/v sodium azide.

2.2 Solid State NMR Sample Preparation

Samples were prepared similarly to a previous protocol [37] with changes for increasing sensitivity [39]. First the 1.2 mL proteoliposome solution is evenly distributed over 40 glass slides (5.7 mm × 10 mm × 0.06–0.08 mm, Marienfeld Scientific, Inc.) and dried in an airtight 0.5 m × 0.5 m × 1.0 m plexi-glass box kept at 22 °C and 98% relative humidity (via a saturated solution of potassium sulfate). Bulk water was visibly removed from the slides after 12–24 h, indicating the formation of a lipid film. 2 μL of deionized water was added to the center of each slide prior to stacking 35 of them on top of each other. The stack was incubated at 37 °C and 98% relative humidity (via a saturated solution of potassium sulfate) in a 1 L glass dessicator. After 3–4 d the stack was then slid into a glass cell (6.4 mm × 4.3 mm × 18 mm, New Era Scientific, Inc.) and sealed with a homemade plastic plug and beeswax (Hampton Research, Inc.) All samples were ~40% w/w buffer determined by weighing the slides and sample cell together before and after the lipid was applied.

2.3 Solid State NMR Spectroscopy

^{1}H-^{15}N SAMPI4 experiments [40] with a 40 μs spin-echo prior to signal acquisition were performed at either 14.1 T or 21.1 T using Low-E probes designed and built at the National High Magnetic Field Laboratory (Tallahassee, Florida). Matching ^{1}H and ^{15}N *rf* fields of 62.5 kHz or 55.6 kHz, recycle delays of 3–5 s and cross polarization times of 1 ms were used. Typically, 28–32 t_1 points were acquired with 3072–5120 transients averaged for each t_1 point.

2.4 PISA Simulations

TM domains were predicted by the TMHMMv2.0 program [41] and manually extended to include probable TM residues at the helix termini. Helical wheels projections were calculated using the online applet from R. Zidovetzki (http://rzlab.ucr.edu/scripts/wheel/wheel.cgi). PISA wheel simulations were performed as previously described [29] using a Matlab (The MathWorks, Inc.) script. ^{15}N chemical shift tensor and ^{1}H-^{15}N dipolar coupling values, obtained from the average of experimental measurements [31], of δ_{11} = 228.1 ppm,

NIH-PA Author Manuscript

NIH-PA Author Manuscript

NIH-PA Author Manuscript

δ_{22} = 81.2 ppm, δ_{33} = 57.3 ppm and d_{HN} = 21470 kHz were used along with standard peptide plane geometry [42] and standard membrane helix torsion angles of φ = −60°, ψ = −45° [43]. The NH-δ_{11} angle used was 17° [44] with δ_{22} perpendicular to the peptide plane. All ^{15}N chemical shifts were referenced externally to saturated solution of ammonium sulfate set to 26.8 ppm. Best-fit PISA wheels were obtained by minimizing the deviation between theoretical and experimental chemical shift and dipolar coupling values while varying tilt and rotation angles. Wave plots were constructed as previously described [26, 45] by plotting the experimental observable versus residue number. A wave with 3.63 residues per repeat was fit to the data. Deviations in rotation angles were determined by calculating the line between the origin of the PISA wheel pattern and the experimental data point and then rotating the predicted resonance along the PISA wheel pattern until the theoretical and experimental values were collinear. The data was presented as Δρ plots [26]. These plots are constructed by normalizing the theoretical and predicted rotation angles between 0° and 360° and then plotted against each other.

3. Results and Discussion

3.1 Helix Tilt Angles

Procedures for assignment of SLF spectra of aligned protein samples combining uniformly and AA specific ^{15}N-labeled samples have been published [26, 32, 46, 47]. The protein under study is complicated by having three helices with similar tilt angles with respect to the bilayer normal or, equivalently, the magnetic field axis. The previously published assignment strategies were not sufficient for Rv1861. Typically the first step for all assignment approaches is to determine the approximate helix tilt angle with respect to the membrane normal using a SLF type spectrum for uniformly ^{15}N-labeled protein. The SAMPI4 [40] result for Rv1861 (Fig. 1a and supplemental Fig. S1) reveals a highly congested spectrum and very few resolved single site resonances. However, the spectrum is that of a well aligned sample and helps restrict the tilt angles of the helices. First, almost all signal intensity lies between 75 and 200 ppm. Second, there is a lack of intensity between 3–6 kHz in the ^{1}H-^{15}N dipolar coupling dimension and between 160–180 ppm in the anisotropic ^{15}N chemical shift dimension resulting in a ‘hole’ in the spectrum. In powder pattern spectra of unaligned proteoliposomes signal intensity is expected in these regions and the absence of it indicates the protein is well aligned in the sample. The spectral intensity in the TM helical region (110–230 ppm anisotropic ^{15}N chemical shift), corresponding to helix tilt angles between 0–50°, can be used to obtain rough estimates of helix tilt angles for this protein. Larger tilt angles would be highly atypical for TM helices. Simulated PISA wheels (Fig. 1b) covering the extremes of the spectral intensity in this region suggest that the three helices of Rv1861 are tilted between 30°–50°, but specific tilt angles cannot be assigned with this data alone. Without a tilt angle or any clearly resolved resonances for each helix, it is impossible to continue the assignment process using established methods.

Before AA specific ^{15}N-labeling, an evaluation of the amino acid composition and sequence is essential. In Fig. 2a the amino acid sequence of the protein including the His_6 tag is shown. Highlighted in red are the residues predicted to be in the TM helices of the protein based on the TMHMMv2.0 program [41]. It should be noted that the prediction can fail to properly detect the end residues for a helix and the result needs to be manually inspected. For example, the C-terminal end of helix one can most likely be extended, see section 3.3. Two-thirds of the backbone amide resonances of the native protein are predicted to be from TM helices, which is consistent with the distribution of intensity in Fig. 1a. Table 1 shows the amino acid content for each predicted helix of Rv1861. The prediction indicates that 12 different amino acids are represented in the helices and the sequences are dominated by glycine and hydrophobic amino acids. Alanine, glycine, and leucine residues are abundant in

NIH-PA Author Manuscript

NIH-PA Author Manuscript

NIH-PA Author Manuscript

all three helices. Conversely, isoleucine, valine, methionine, phenylalanine, tryptophan, serine and tyrosine are either absent from one helix or, in the case of the abundant isoleucine and valine residues, mostly in two helices with only one residue in the third helix.

Helical wheel projections (Fig. 2b) provide a visualization of the distribution of the amino acid residues around the helix, if it is assumed for the time being that the helices have regular structure with constant tilt and rotation angles throughout. The distribution of certain amino acids in the helical wheel defines a pattern for a PISA wheel that can be used to interpret AA specific ^{15}N-labeled spectra. First, alanine residues (Fig. 2b, red circles), with one exception, reside on only one side of each helix. Second, inspection of the helical wheels for leucine residues (Fig. 2b, cyan circles) reveals that, with the exception of the C-terminal end of helix two, leucine residues also cover only one side of each helix. Third, valine residues (Fig. 2b, gray circles), the second most common amino acid residue in the TM helices, are distributed over almost all faces of helices two and three but not helix one. The resonance patterns expected in SLF spectra for helices can be predicted based on the helical wheel patterns, making these properties of the protein sequence a useful lens by which AA specific labeled data can be interpreted.

AA specific ^{15}N-labeling is typically used to fix the tilt and rotation angles for each helix. The spectrum of the uniformly labeled sample suggested that helical tilts would be greater than or equal to 30°. In addition, it is difficult to imagine from the positions of the charged and highly polar residues in the primary sequence (Fig. 2a) that any of the helices would be longer than 26 residues. A 26 residue helix would not have sufficient length to span the ~30 Å hydrophobic dimension of the DMPC/DMPG bilayer [48, 49] if the tilt angle was greater than 50°. Based on the primary sequence analysis, the key valine, alanine and leucine labeled samples were collected first to confirm the range of tilt angles suggested by the uniformly labeled spectrum. Valine was chosen as an abundant amino acid label to report on the tilt angle for helix two and three while leucine and alanine were chosen because they cover opposing faces of each helix and therefore should provide an upper and lower bound for the helix tilt angles. For Rv1861, these residues account for more than a third of the predicted TM helix residues. The spectra (Figs. 2c and 2d) confirm that the helical tilts range between 30° and 50° and suggest that tilts greater than 45° are unlikely. These three spectra alone reveal well resolved resonances for 30 of the 33 expected valine, leucine, and alanine resonances from Rv1861. One leucine and two alanine resonances are anticipated to be in the highly dynamic N-terminal segment, resulting in their absence due to weak cross-polarization. The lineshapes exhibited for these spectra (Figs. 2c and 2d) reveal that the protein alignment is excellent with a mosaic spread of ~1° [50]. The alanine and leucine resonances are distributed on opposing sides of the TM spectral domain centered around ~165 ppm, while the valine resonances seem to be scattered over the entire TM spectral domain occupied by the alanine and leucine resonances. These distributions indicate that the three helices have similar tilt angles and are consistent with the patterns suggested by the primary sequence prediction and helical wheel analysis.

3.2 Helix Rotation Angles

To identify which resonances belong to each helix and fix the helix rotation angles, SAMPI4 experiments were collected on additional AA specific ^{15}N-labeled samples that cover most of the remaining TM hydrophobic residues of Rv1861 (isoleucine, phenylalanine, and tryptophan). In order to make sequence specific assignments, a strategy was devised utilizing the unequal distribution of the common amino acids (isoleucine, leucine and valine) in the core region of each helix combined with amino acids not common in one or more helices (alanine, phenylalanine and tryptophan). Focus is paid to residues that span all 360° of rotational space in the core region and consequently 360° around the predicted PISA wheel for each helix. Theoretical PISA wheel patterns are calculated for tilt and rotation

NIH-PA Author Manuscript

NIH-PA Author Manuscript

NIH-PA Author Manuscript

angles between 30–45° and 0–360°, respectively, and compared to the experimental data. The tilt and rotation angles that best matched the predicted core residues with the experimental data were then chosen as initial orientations for each helix. Fig. 3a and 3b illustrate how the tilt and rotation angles are defined. The tilt angle is defined between the vectors **n** and **h** (membrane normal and helix axis, respectively) while the rotation angle is defined as a right hand rotation around **h**. Vector **o** defines the origin for the rotation angle and is in the plane formed by **n** and **h**. The positions of the rotation angles for the first residue (ρ_0) of each helix are depicted at the base of the cylinder in Fig. 3a and on a 40° PISA wheel in Fig. 3b (see section 3.3).

Best-fit PISA patterns and initial tilt and rotation angles are shown in Figs. 4d, 4e and 4f for helix one, two and three, respectively. For helix one (Figs. 4a, 4d and 4g) isoleucine and tryptophan residues are in the core and used for the assignment strategy. Although the abundance of glycine residues in the TM helices makes them important, we were unable to specifically label these residues despite considerable efforts and various strategies, making it impossible to utilize them for assignments. Notice that the tryptophan spectrum has very strong resonances observed for each of the four indoles – the higher intensity of the indole resonances compared to the amide resonances is a property that we have observed in other proteins as well. Three isoleucine resonances (I26, I28 and I41) coupled with W34 indicated by solid arrows in Figs. 4a and 4g and were chosen as the best match to the prediction in Fig. 3d. The pattern best fits to a PISA wheel with a tilt angle of 38° and a rotation angle of 65°, where the rotation angle is defined relative to the position of I20. The core of helix two, Figs. 4b, 4e and 4h, is defined by five valine and two alanine sites (again not counting the abundant glycine residues) that form a PISA pattern that best fits the data with tilt and rotation angles of 41° and 140°, respectively. The rotation angle here is defined relative to I47. These resonances are indicated by solid arrows in Figs. 4b and 4h which compare well with the predicted resonances in Fig. 4e. Helix three has two phenylalanine and three leucine residues that define its core with a best fit to the experimental data using a PISA wheel with helix tilt and rotation angles of 44° and 70°, respectively, having the rotation defined relative to W78. The PISA pattern is presented in Fig. 4f and the assigned resonances indicated with arrows in Figs. 4c and 4i. Data with representative 1D slices are presented in Supplemental Fig. S1.

3.3 Full Assignments and Model Assessment

Starting with the initial core assignments for each helix, the full PISA patterns covering all core residues that were labeled, excluding the first and last six residues in the primary sequence of each helix, were compared to the remaining unassigned resonances from the AA specific ^{15}N-labeled spectra. More assignments could be made with high assurance, such as A32 (4.6 kHz and 135.7 ppm), L35 (8.1 kHz and 159.9 ppm), I53 (3.5 kHz and 194.0 ppm), F59 (0.8 kHz and 123.0 ppm), A88 (0.7 kHz and 152.6 ppm), and V90 (4.0 kHz and 119.8 ppm). For the full list of the extended core region assignments see the bold font residues in Table 2. Based on these high confidence core assignments, refined PISA wheels were calculated by performing a root mean square minimization with respect to deviations in dipolar coupling and anisotropic ^{15}N chemical shift, in much the same way they would be using existing computational approaches [31–33]. The tilt and rotation angles are presented in Table 3. Next, the resonances for these high confidence assignments were removed from consideration and resonances belonging to the end of each helix were assigned. Since we were including resonances from the termini of each helix, a methionine labeled sample was also utilized (Supplemental Fig. S1). This latter data set is similar to previously published data [37]. Although these remaining resonances exhibited larger deviations from the predicted values than those from the core regions, removal of more than half of the resonances from each spectrum (i.e. the extended core assignments) greatly simplified the

NIH-PA Author Manuscript

NIH-PA Author Manuscript

NIH-PA Author Manuscript

assignment of the remaining resonances. Complete assignments for the observed residues of each helix are presented in Table 2.

One way to evaluate the assignments and the plausibility of the orientational model for each helix is through wave plots [33, 45, 51] of the chemical shifts and dipolar couplings. These plots illustrate both the degree of uniformity of the helix while also identifying significant deviations from ideal helical structure along the length of the helix by plotting the experimental data as a function of residue number. The result for each helix of Rv1861 is shown in Fig. 5. The wave plots confirm that the protein has regular helical structure throughout the core region of each helix and that the tilt and rotation angles are constant throughout the length of each helix. Not surprisingly, the dipolar coupling data fit better than the chemical shift data, as it is well known that the chemical shift tensor element magnitudes vary along the amino acid sequence [52, 53]. The termini defined by the first and last six residues of each helix fit less well and the labeled sites in this region show substantial deviations in either anisotropic ^{15}N chemical shift, dipolar coupling or both. Slight changes in peptide plane tilt relative to the helix axis (nominally 8° for TM helices) result in a significant dispersion for the anisotropic ^{15}N chemical shifts (~15 ppm) and somewhat less dispersion for the dipolar couplings (~1 kHz) that can account for the observed scatter in the experimental data relative to the theoretical waves [44] without disrupting the regular helical structure for each helix. It is important to note that the error bars in Fig. 5 represent error in the measurement of the experimental value and it should not be alarming that the error does not overlap with the prediction for some sites, even in the core region. The significance of the observation of a PISA pattern should not be understated. Based on published calculations [44] changes in helix or ψ angles greater than ±4° would obliterate the PISA pattern. Since we observe the PISA patterns, dipolar waves and chemical shift waves here, the limits for the and ψ torsion angle variation are ±4° for the core regions and ±8° for the helix termini. These limits indicate that the helical structures are indeed quite uniform.

The wave plots are highly sensitive to changes in tilt angle and a series of deviations for one part of a helix [54] can suggest a kink in the helix resulting in a change in tilt angle. Changes in tilt for a portion of the helix would result in a break in the wave pattern and a shift in both the magnitude and the central frequency (in kHz or ppm) of the oscillation. Deviations from the rotational angle would manifest as a break in the periodicity of the oscillation, such as the influence of a π-bulge, where another residue is inserted into the helix (e.g. Bacteriorhodopsin [55]). Based on the dipolar and chemical shift waves, neither of these distortions in the wave pattern occurs in the helix core regions. Helix one, may have a slight change in tilt at each end as indicated by deviations towards smaller anisotropic ^{15}N chemical shift for the sites in the termini of the helix. However, no such convincing deviation is seen in the corresponding dipolar wave for helix one. Consequently, the spectral dispersion provided by a few degree change in the peptide plane tilt angle is more likely for these sites than a change in the global helix tilt angle. The C-terminus of helix two presents a somewhat different deviation from the ideal pattern in which the anisotropic ^{15}N chemical shifts are both larger and smaller than the predicted values. This is typical of an increased tilt of the peptide planes relative to the helix axis as the helix gains access to water near the edge of the hydrophobic region of the bilayer. Water soluble helices have average peptide plane tilt angles of 12° instead of 8°. This relatively small change in tilt for peptide planes is facilitated by decreased stability resulting from having only a single hydrogen bond per peptide plane. As previously stated, the change in peptide plane tilt can account for a 15 ppm change in the chemical shift away from the average value for a helix tilted at ~40° [44]. Many sites in the helix three core region exhibit small deviations (both higher and lower) in anisotropic ^{15}N chemical shift. Regardless, the minimization procedure always converges on the same tilt and rotation angles. In light of the dipolar coupling data that fit well over

NIH-PA Author Manuscript

NIH-PA Author Manuscript

NIH-PA Author Manuscript

residues W78-I94, these deviations are best interpreted as slight changes in peptide plane tilt angles in an otherwise regular helix three.

Not all significant deviations are found in the termini of a helix. For example, V89 resides in the core of helix three with substantial deviations in both chemical shift and dipolar coupling suggesting structural distortion at this site. Although the chemical shifts of the terminal residues following this site (V95, M97 and V98) fit well to the wave, the dipolar coupling data does not fit as well which suggests that this section of helix is slightly distorted. Interestingly, the few sites from the core residues in helix one and three that deviate significantly from the theoretical ^{1}H-^{15}N dipolar coupling pattern are either in the middle of a GxIxG motif, as for I31 in Fig. 5a, or next to an AxxxAV motif, as for V89 in Fig. 5c. These motifs can also be seen in the primary sequence in Fig. 2a and are known to provide surfaces for close helix-helix association [56–60] which may cause deviations from ideal helix geometry. Overall, the wave analysis indicates a well-fitting model with constant tilt and rotation angles for all three helices. Deviations from the model are explained by helix packing interfaces in the core region or slight disruption of the helix structure at the termini.

While helix tilt and gross changes in rotational angle are well assessed in the wave plots, the graphs of experimental versus predicted rotational angles, known as $\Delta\rho$ plots [26] report on deviations from the ideal rotation around the helix axis per residue of ~100° (Fig. 6). The core residues are shown in solid circles, while the terminal residues are shown in open circles. Almost all core region sites for all three helices are within ±15° of the predicted values and further confirm the regular helical structure of the core region. Additionally, the experimental ρ angles are both greater and lesser than the predicted value along the length of the helices. The values above and below the diagonal line represent a compensating pattern for the rho values further indicating that the α-helical structure is maintained throughout each sequence. As we saw with the wave plots, the core region of helix three is the most distorted of the helices. Here, there are three residues that have a deviation between 15° and 30° and two sites with larger than 30° deviations. These larger exceptions are A84 and A88, which form an AxxxA motif (see Fig. 2a). It should be noted that these sites follow the wave patterns in Figs. 5c and 5f closely. However, the neighboring V89 site has the only significant deviation in the wave plots for the core residues but displays a change in rotation angle of only 12°, suggesting these deviations are structurally related. Combined with the regular helical structure of the surrounding core residues, these three sites (A84, A88 and V89) indicate that there must be some localized, but self-compensating distortion of the structure in this region of helix three.

3.4 Deviations from Ideal Helices and Tertiary Structure Implications

While no inter-helical restraints were measured to determine the tertiary structure of the protein, conclusions can still be made about helix association in the tertiary structure. The orientation (tilt and rotation angle) for each helix relative to the bilayer normal is known from the OS ssNMR data. Also, with the exception of a few angstroms of vertical translational movement in the bilayer and rotation about the bilayer normal, the structure and position in the bilayer of each helix is fixed. Furthermore, the C_α and C_β positions are restrained by tetrahedral geometry so the surface for glycine and alanine residues is well defined by the backbone torsion angles, that are based on the helical structures characterized here and restricted to ±4° for core regions and ±8° for helix termini. Interestingly, each helix has multiple glycine and alanine residues providing potential helix-helix interaction surfaces (see the helical models in Fig. 7 and the primary sequence in Fig. 2a). Rather surprisingly, there are four GG pairs in the protein sequence (see Fig. 2a), two of them appear near the N-termini of helices one and three and most likely participate in helix termination. More interesting are the GG pairs in the middle of helices one and three (Fig. 7a and 7c) which do not appear to kink or distort their respective helices in any way. It may be that in a different

NIH-PA Author Manuscript

NIH-PA Author Manuscript

NIH-PA Author Manuscript

functional state these helices actually take on a distorted conformation facilitated by these residues, but here they do not induce a change in tilt or rotational orientation of the helices.

3.5 Data Quality

As the number of TM helices increases, the SLF spectra of uniformly aligned helical membrane proteins becomes increasingly complex and congested. While the spectra from small proteins with one or two helices have shown excellent lineshapes in the literature, it was not clear if larger proteins would. Larger structures might exhibit more dynamics leading to decreased signal intensity or broader lines in the SLF spectra. The data for Rv1861 shows that all of the labeled TM amide sites are observed with excellent lineshapes suggesting that a protein with three TM helices can have sufficiently narrow resonances to allow complete TM assignments. The only sites for which a resonance is not observed reside in either a loop or in the protein termini. TM helices have been shown to be quite uniform due to increased hydrogen bonding strength in the hydrophobic core of lipid bilayers [43, 44]. However, this is the first time that SLF experiments have been obtained on a protein with so many glycine residues (23% of the predicted amino acid composition of the helices). Glycine is a known helix breaking residue and the helical structures may be less stable and less uniform for Rv1861 than for some other helical membrane proteins having fewer glycine residues. Here, the helices have regular α-helical structure with constant tilt and rotation angles but there are clearly small, but significant, structural perturbations, especially along helix three. Importantly, PISA patterns are maintained for the length of each helix and it should be stressed how this indicates the helices are unbent and have minimal deviation from ideal membrane protein α-helical torsion angles ($\varphi=-60°$ and $\psi=-45°$). Finally, tryptophan residues are important structural features of membrane proteins. Here, resonances for both the backbone and sidechain sites are observed for the four tryptophans in Rv1861. Although not described here, the high quality of the data would permit the characterization of the sidechain orientations for these sites in addition to the backbone conformation once the indole resonances are assigned and their dynamics evaluated.

3.6 New Approach to Assigning OS ssNMR Data

When more than one TM helix is present, and especially if the tilt angles are small or similar, an ambiguity will be introduced in the assignments between the helices. Assigning resonances sequentially (i.e. *i*, *i*+1) based on helical geometry is therefore difficult. Here, we have tackled this issue by focusing instead on the distribution of common and uncommon amino acids in each helical sequence. Unique patterns that cover the core region of each helix are used to identify the approximate tilt and rotation angles. These patterns are much easier to observe in the sparse AA specific ^{15}N-labeled spectra of the protein. After the core region residues were removed from consideration, the remaining residues were easily assigned. Although primarily helical, the terminal regions display more structural perturbations from the influence of water and membrane interfacial region. In the core region there are clear, specific, structural perturbations of individual peptide planes that appear to be self-compensating allowing for the helices to have regular structure. The strength of our strategy is that it does not require completely ideal helical structure for the determination of complete assignments. Furthermore, the results are all based on 2D spectra that are relatively simple to obtain.

4. Conclusions

In conclusion, we have shown that TM resonance assignments can be made for a three TM helix membrane protein in a lipid bilayer environment using OS ssNMR, even when the PISA wheels severely overlap. The strategy described here is generally applicable to other proteins of similar size. The information obtained is valuable in light of the scant structural

NIH-PA Author Manuscript

NIH-PA Author Manuscript

NIH-PA Author Manuscript

characterizations for membrane proteins similar in size to Rv1861 and the high genomic content for similar proteins (e.g. ~50% of all *Mtb* membrane proteins have between one to three TM helices [61]). Although not a tertiary structure, the results constrain the global TM structure at high resolution by defining precise tilt and rotation angles which severely constrain the possible packing arrangements for the helices. More importantly, high resolution orientational restraints for the peptide planes of each TM helix are obtained which reduce the number of distance restraints that must be measured to calculate a tertiary structure. Furthermore, tertiary modeling efforts using established methods (e.g. HADDOCK [62]) can readily be applied. It is now possible to routinely assign spectra of proteins with up to three TM helices and hence the majority of membrane proteins in bacterial genomes.

Supplementary Material

Refer to Web version on PubMed Central for supplementary material.

Acknowledgments

The authors wish to thank, Bill Brey, Perter Gor'kov and Jason Kitchen of the RF Group at the NHMFL for invaluable assistance with the 21.1 T magnet and probe technology. Huajun Qin provided invaluable assistance with protein expression and purification. The work was made possible by grants from the National Institute of Allergy and Infectious Diseases (5R01-A1073891 and P01A1074805) and the use of the National High Magnetic Field Laboratory, a cooperative agreement between the State of Florida and the National Science Foundation (DMR- 1157490).

References

1. Anfinsen CB. Principles That Govern Folding of Protein Chains. Science. 1973; 181:223–230. [PubMed: 4124164]
2. Zhou HX, Cross TA. Modeling the membrane environment has implications for membrane protein structure and function: Influenza A M2 protein. Protein Science. 2013; 22:381–394. [PubMed: 23389890]
3. Zhou H-X, Cross TA. Influences of Membrane Mimetic Environments on Membrane Protein Structures. Annual Review of Biophysics. 2013; 42:361–392.
4. Cross TA, Murray DT, Watts T. Helical membrane protein conformations and their environment. European Biophysical Journal. 201310.1007/s00249-00013-00925-x
5. Zheng J, Jia Z. Structural biology: Tiny enzyme uses context to succeed. Nature. 2013; 497:445–446. [PubMed: 23676672]
6. Cross TA, Sharma M, Yi M, Zhou HX. Influence of solubilizing environments on membrane protein structures. Trends in Biochemical Sciences. 2011; 36:117–125. [PubMed: 20724162]
7. Zoonens M, Comer J, Masscheleyn S, Pebay-Peyroula E, Chipot C, Miroux B, Dehez F. Dangerous Liaisons between Detergents and Membrane Proteins. The Case of Mitochondrial Uncoupling Protein 2. Journal of the American Chemical Society. 2013; 135:15174–15182. [PubMed: 24021091]
8. Torres J, Stevens TJ, Samso M. Membrane proteins: the 'Wild West' of structural biology. 2003; 28:137–144.
9. Dong H, Sharma M, Zhou HX, Cross TA. Glycines: role in alpha-helical membrane protein structures and a potential indicator of native conformation. Biochemistry. 2012; 51:4779–4789. [PubMed: 22650985]
10. Zhou HX, Cross TA. Influences of Membrane Mimetic Environments on Membrane Protein Structures. Annual review of biophysics. 2013; 42:361–392.
11. Zhou HX, Cross TA. Modeling the membrane environment has implications for membrane protein structure and function: Influenza A M2 protein. Protein Science. 2013; 22:381–394. [PubMed: 23389890]

NIH-PA Author Manuscript NIH-PA Author Manuscript NIH-PA Author Manuscript

12. Van Horn WD, Kim HJ, Ellis CD, Hadziselimovic A, Sulistijo ES, Karra MD, Tian C, Sonnichsen FD, Sanders CR. Solution nuclear magnetic resonance structure of membrane-integral diacylglycerol kinase. Science. 2009; 324:1726–1729. [PubMed: 19556511]
13. OuYang B, Xie S, Berardi MJ, Zhao X, Dev J, Yu W, Sun B, Chou JJ. Unusual architecture of the p7 channel from hepatitis C virus. Nature. 2013; 498:521–525. [PubMed: 23739335]
14. Tang M, Nesbitt AE, Sperling LJ, Berthold DA, Schwieters CD, Gennis RB, Rienstra CM. Structure of the Disulfide Bond Generating Membrane Protein DsbB in the Lipid Bilayer. Journal of Molecular Biology. 2013; 425:1670–1682. [PubMed: 23416557]
15. Walz T, Hirai T, Murata K, Heymann JB, Mitsuoka K, Fujiyoshi Y, Smith BL, Agre P, Engel A. The three-dimensional structure of aquaporin-1. Nature. 1997; 387:624–627. [PubMed: 9177353]
16. Kebbel F, Kurz M, Arheit M, Gruetter MG, Stahlberg H. Structure and Substrate-Induced Conformational Changes of the Secondary Citrate/Sodium Symporter CitS Revealed by Electron Crystallography. Structure. 2013; 21:1243–1250. [PubMed: 23810698]
17. Benlekbir S, Bueler SA, Rubinstein JL. Structure of the vacuolar-type ATPase from Saccharomyces cerevisiae at 11-angstrom resolution. Nature Structural and Molecular Biology. 2012; 19:1356–1362.
18. Cady SD, Mishanina TV, Hong M. Structure of Amantadine-Bound M2 Transmembrane Peptide of Influenza A in Lipid Bilayers from Magic-Angle-Spinning Solid-State NMR: The Role of Ser31 in Amantadine Binding. Journal of Molecular Biology. 2009; 385:1127–1141. [PubMed: 19061899]
19. Can TV, Sharma M, Hung I, Gor'kov PL, Brey WW, Cross TA. Magic Angle Spinning and Oriented Sample Solid-State NMR Structural Restraints Combine for Influenza A M2 Protein Functional Insights. Journal of the American Chemical Society. 2012; 134:9022–9025. [PubMed: 22616841]
20. Das BB, Nothnagel HJ, Lu GJ, Son WS, Tian Y, Marassi FM, Opella SJ. Structure Determination of a Membrane Protein in Proteoliposomes. Journal of the American Chemical Society. 2012; 134:2047–2056. [PubMed: 22217388]
21. Park SH, Das BB, Casagrande F, Tian Y, Nothnagel HJ, Chu MN, Kiefer H, Maier K, De Angelis AA, Marassi FM, Opella SJ. Structure of the chemokine receptor CXCR1 in phospholipid bilayers. Nature. 2012; 491:779–783. [PubMed: 23086146]
22. Park SH, De Angelis AA, Nevzorov AA, Wu CH, Opella SJ. Three-dimensional structure of the transmembrane domain of Vpu from HIV-1 in aligned phospholipid bicelles. Biophysical Journal. 2006; 91:3032–3042. [PubMed: 16861273]
23. Sharma M, Yi MG, Dong H, Qin HJ, Peterson E, Busath DD, Zhou HX, Cross TA. Insight into the Mechanism of the Influenza A Proton Channel from a Structure in a Lipid Bilayer. Science. 2010; 330:509–512. [PubMed: 20966252]
24. Thiriot DS, Nevzorov AA, Zagyanskiy L, Wu CH, Opella SJ. Structure of the coat protein in Pf1 bacteriophage determined by solid-state NMR Spectroscopy. Journal of Molecular Biology. 2004; 341:869–879. [PubMed: 15288792]
25. Murray DT, Das N, Cross TA. Solid State NMR Strategy for Characterizing Native Membrane Protein Structures. Accounts of Chemical Research. 2013; 46:2172–2181. [PubMed: 23470103]
26. Wang JF, Kim S, Kovacs F, Cross TA. Structure of the transmembrane region of the M2 protein H + channel. Protein Science. 2001; 10:2241–2250. [PubMed: 11604531]
27. Hou GJ, Paramasivam S, Yan S, Polenova T, Vega AJ. Multidimensional Magic Angle Spinning NMR Spectroscopy for Site-Resolved Measurement of Proton Chemical Shift Anisotropy in Biological Solids. Journal of the American Chemical Society. 2013; 135:1358–1368. [PubMed: 23286322]
28. Vosegaard T, Kamihira-Ishijima M, Watts A, Nielsen NC. Helix conformations in 7TM membrane proteins determined using oriented-sample solid-state NMR with multiple residue-specific N-15 labeling. Biophysical Journal. 2008; 94:241–250. [PubMed: 17827220]
29. Denny JK, Wang JF, Cross TA, Quine JR. PISEMA powder patterns and PISA wheels. Journal of Magnetic Resonance. 2001; 152:217–226. [PubMed: 11567575]
30. Marassi FM, Opella SJ. A solid-state NMR index of helical membrane protein structure and topology. Journal of Magnetic Resonance. 2000; 144:150–155. [PubMed: 10783285]

NIH-PA Author Manuscript NIH-PA Author Manuscript NIH-PA Author Manuscript

31. Wang J, Denny J, Tian C, Kim S, Mo Y, Kovacs F, Song Z, Nishimura K, Gan Z, Fu R, Quine JR, Cross TA. Imaging membrane protein helical wheels. Journal of Magnetic Resonance. 2000; 144:162–167. [PubMed: 10783287]
32. Marassi FM, Opella SJ. Simultaneous assignment and structure determination of a membrane protein from NMR orientational restraints. Protein Science. 2003; 12:403–411. [PubMed: 12592011]
33. Kovacs FA, Denny JK, Song Z, Quine JR, Cross TA. Helix tilt of the M2 transmembrane peptide from influenza A virus: an intrinsic property. Journal of Molecular Biology. 2000; 295:117–125. [PubMed: 10623512]
34. Tang W, Knox RW, Nevzorov AA. A spectroscopic assignment technique for membrane proteins reconstituted in magnetically aligned bicelles. Journal of Biomolecular NMR. 2012; 54:307–316. [PubMed: 22976525]
35. Mote KR, Gopinath T, Traaseth NJ, Kitchen J, Gor'kov PL, Brey WW, Veglia G. Multidimensional oriented solid-state NMR experiments enable the sequential assignment of uniformly N-15 labeled integral membrane proteins in magnetically aligned lipid bilayers. Journal of Biomolecular NMR. 2011; 51:339–346. [PubMed: 21976256]
36. Marmiesse M, Brodin P, Buchrieser C, Gutierrez C, Simoes N, Vincent V, Glaser P, Cole ST, Brosch R. Macro-array and bioinformatic analyses reveal mycobacterial 'core' genes, variation in the ESAT-6 gene family and new phylogenetic markers for the Mycobacterium tuberculosis complex. Microbiology. 2004; 150:483–496. [PubMed: 14766927]
37. Li CG, Gao P, Qin HJ, Chase R, Gor'kov PL, Brey WW, Cross TA. Uniformly aligned full-length membrane proteins in liquid crystalline bilayers for structural characterization. Journal of the American Chemical Society. 2007; 129:5304–5305. [PubMed: 17407289]
38. Page RC, Moore JD, Nguyen HB, Sharma M, Chase R, Gao FP, Mobley CK, Sanders CR, Ma L, Sonnichsen FD, Lee S, Howell SC, Opella SJ, Cross TA. Comprehensive evaluation of solution nuclear magnetic resonance spectroscopy sample preparation for helical integral membrane proteins. Journal of Structural and Functional Genomics. 2006; 7:51–64. [PubMed: 16850177]
39. Das N, Murray DT, Cross TA. Lipid bilayer preparations of membrane proteins for oriented and magic-angle spinning solid-state NMR samples. Nature Protocols. 201310.1038/nprot.2013.1129
40. Nevzorov AA, Opella SJ. Selective averaging for high-resolution solid-state NMR spectroscopy of aligned samples. Journal of magnetic resonance (San Diego, Calif: 1997). 2007; 185:59–70.
41. Sonnhammer EL, von Heijne G, Krogh A. A hidden Markov model for predicting transmembrane helices in protein sequences. Proceedings: International Conference on Intelligent Systems for Molecular Biology. 1998; 6:175–182.
42. Engh RA, Huber R. Accurate Bond and Angle Parameters for X-Ray Protein-Structure Refinement. Acta Crystallographica Section A. 1991; 47:392–400.
43. Kim S, Cross TA. Uniformity, ideality, and hydrogen bonds in transmembrane alpha-helices. Biophysical Journal. 2002; 83:2084–2095. [PubMed: 12324426]
44. Page RC, Kim S, Cross TA. Transmembrane helix uniformity examined by spectral mapping of torsion angles. Structure. 2008; 16:787–797. [PubMed: 18462683]
45. Mesleh MF, Veglia G, DeSilva TM, Marassi FM, Opella SJ. Dipolar waves as NMR maps of protein structure. Journal of the American Chemical Society. 2002; 124:4206–4207. [PubMed: 11960438]
46. Traaseth NJ, Buffy JJ, Zamoon J, Veglia G. Structural dynamics and topology of phospholamban in oriented lipid bilayers using multidimensional solid-state NMR. Biochemistry. 2006; 45:13827–13834. [PubMed: 17105201]
47. De Angelis AA, Howell SC, Nevzorov AA, Opella SJ. Structure determination of a membrane protein with two trans-membrane helices in aligned phospholipid bicelles by solid-state NMR spectroscopy. Journal of the American Chemical Society. 2006; 128:12256–12267. [PubMed: 16967977]
48. Li C, Yi M, Hu J, Zhou HX, Cross TA. Solid-state NMR and MD simulations of the antiviral drug amantadine solubilized in DMPC bilayers. Biophysical Journal. 2008; 94:1295–1302. [PubMed: 17890391]

NIH-PA Author Manuscript

NIH-PA Author Manuscript

NIH-PA Author Manuscript

49. Petrache HI, Tristram-Nagle S, Nagle JF. Fluid phase structure of EPC and DMPC bilayers. Chemistry and Physics of Lipids. 1998; 95:83–94. [PubMed: 9807810]
50. Quine JR, Achuthan S, Asbury T, Bertram R, Chapman MS, Hu J, Cross TA. Intensity and mosaic spread analysis from PISEMA tensors in solid-state NMR. Journal of Magnetic Resonance. 2006; 179:190–198. [PubMed: 16413215]
51. Mesleh MF, Lee S, Veglia G, Thiriot DS, Marassi FM, Opella SJ. Dipolar waves map the structure and topology of helices in membrane proteins. Journal of the American Chemical Society. 2003; 125:8928–8935. [PubMed: 12862490]
52. Poon A, Birn J, Ramamoorthy A. How does an amide-(15)N chemical shift tensor vary in peptides? Journal of Physical Chemistry B. 2004; 108:16577–16585.
53. Saito H, Ando I, Ramamoorthy A. Chemical shift tensor - The heart of NMR: Insights into biological aspects of proteins. Progress in Nuclear Magnetic Resonance Spectroscopy. 2010; 57:181–228. [PubMed: 20633363]
54. Hu J, Asbury T, Achuthan S, Li CG, Bertram R, Quine JR, Fu RQ, Cross TA. Backbone structure of the amantadine-blocked trans-membrane domain M2 proton channel from influenza A virus. Biophysical Journal. 2007; 92:4335–4343. [PubMed: 17384070]
55. Luecke H, Schobert B, Richter HT, Cartailler JP, Lanyi JK. Structure of bacteriorhodopsin at 1.55 angstrom resolution. J Mol Biol. 1999; 291:899–911. [PubMed: 10452895]
56. Kairys V, Gilson MK, Luy B. Structural model for an AxxxG-mediated dimer of surfactant-associated protein C. European Journal of Biochemistry. 2004; 271:2086–2092. [PubMed: 15153098]
57. Kleiger G, Grothe R, Mallick P, Eisenberg D. GXXXG and AXXXA: common alpha-helical interaction motifs in proteins, particularly in extremophiles. Biochemistry. 2002; 41:5990–5997. [PubMed: 11993993]
58. Langosch D, Heringa J. Interaction of transmembrane helices by a knobs-into-holes packing characteristic of soluble coiled coils. Proteins: Structure, Function, and Bioinformatics. 1998; 31:150–159.
59. MacKenzie KR, Prestegard JH, Engelman DM. A transmembrane helix dimer: Structure and implications. Science. 1997; 276:131–133. [PubMed: 9082985]
60. Smith SO, Song D, Shekar S, Groesbeek M, Ziliox M, Aimoto S. Structure of the transmembrane dimer interface of glycophorin A in membrane bilayers. Biochemistry. 2001; 40:6553–6558. [PubMed: 11380249]
61. Qin H, Hu J, Hua Y, Challa SV, Cross TA, Gao FP. Construction of a series of vectors for high throughput cloning and expression screening of membrane proteins from Mycobacterium tuberculosis. BMC Biotechnology. 2008; 8
62. Dominguez C, Boelens R, Bonvin AM. HADDOCK: a protein-protein docking approach based on biochemical or biophysical information. J Am Chem Soc. 2003; 125:1731–1737. [PubMed: 12580598]

NIH-PA Author Manuscript

NIH-PA Author Manuscript

NIH-PA Author Manuscript

Highlights

- Separated local field experiments applied to a three helix, full-length, membrane protein.
- Amino acid specific ^{15}N-labeling resolves all labeled transmembrane resonances.
- A new assignment strategy is shown to assign all ^{15}N-labeled transmembrane sites.
- Assignment strategy based on unique, core region, residues of each helix.

NIH-PA Author Manuscript

NIH-PA Author Manuscript

NIH-PA Author Manuscript

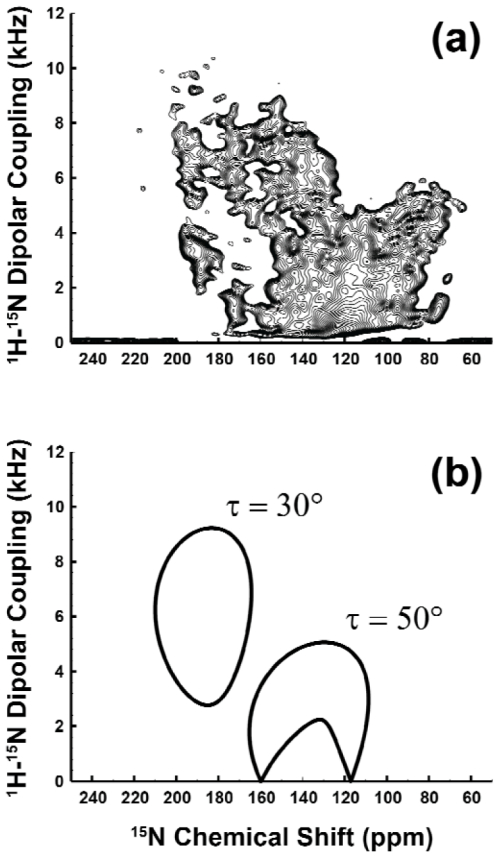

Fig. 1.

(a) Uniformly 15N-labeled Rv1861 SAMPI4 spectrum is consistent with the 30–50° theoretical PISA wheels in (b). 75 contours starting at 1.4σ and increasing by a factor of 1.1 are shown in (a).

NIH-PA Author Manuscript

NIH-PA Author Manuscript

NIH-PA Author Manuscript

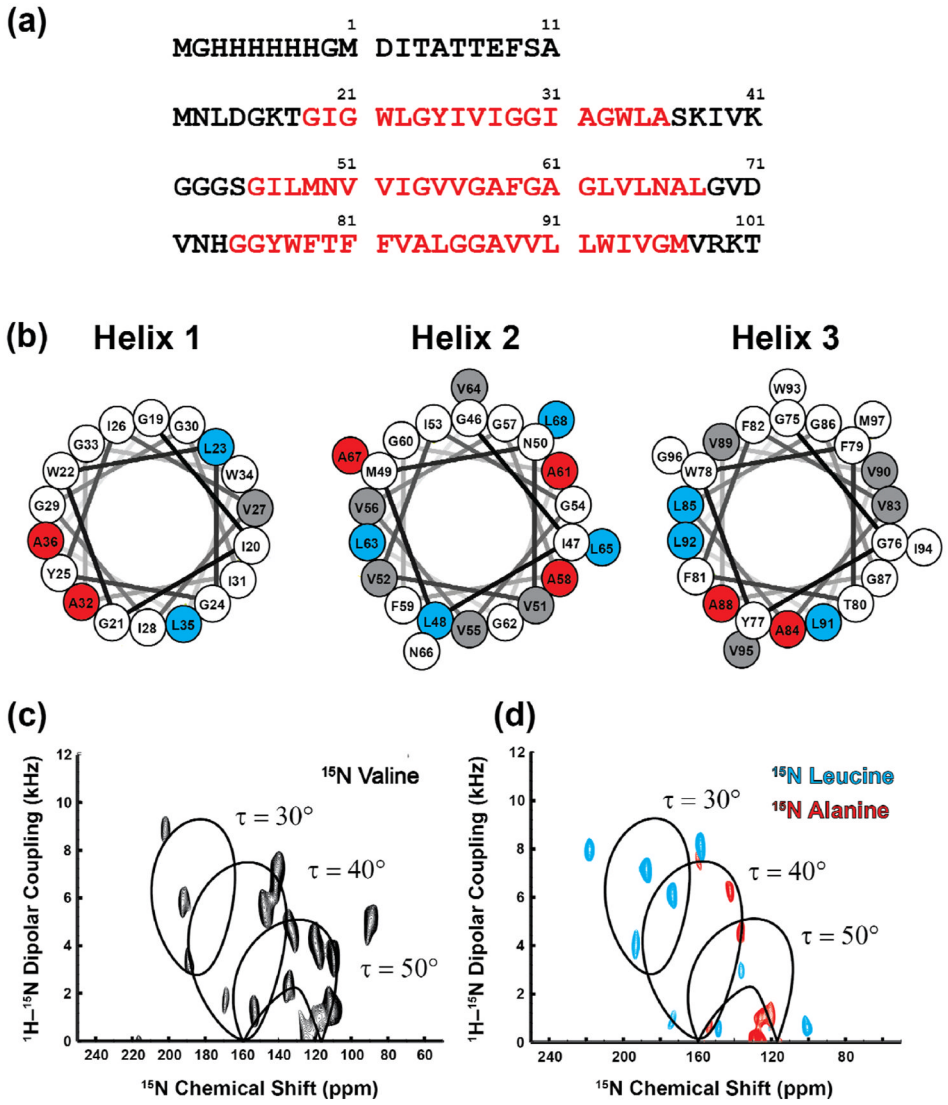

Fig. 2.

Sequence analysis and refinement of tilt angles. (a) Primary sequence of Rv1861. TM helix domains predicted by TMHMMv2.0 are highlighted in red. (b) Helical wheel projections for each predicted helix of Rv1861. Valine residues are highlighted in gray, alanine residues in red and leucine residues in cyan. (c) and (d) SAMPI4 Rv1861 spectra of ^{15}N-valine, (c) black, and ^{15}N-leucine, (d) cyan, or ^{15}N-alanine, (d) red, labeled samples overlayed with PISA wheels between 30, 40 and 50° tilt angles. 30 contours starting at 4σ, 9σ, and 6σ and increasing by 1.05 are shown for Valine, Leucine and Alanine, respectively.

NIH-PA Author Manuscript

NIH-PA Author Manuscript

NIH-PA Author Manuscript

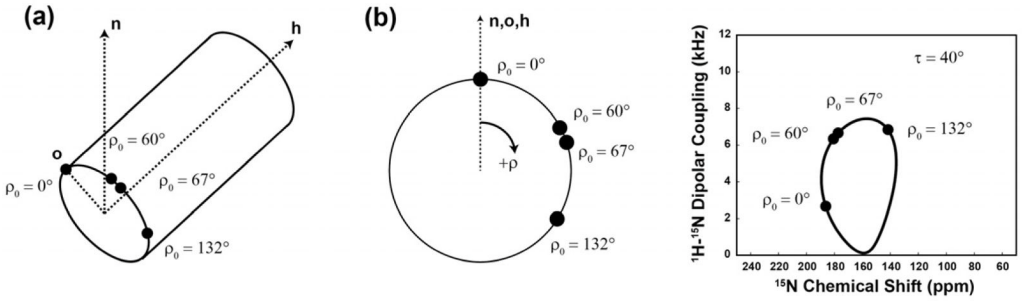

Fig. 3.

Definition of tilt and rotation angles. (a) Cylindrical representation of a helix. **n** is the membrane normal, **h** is the helix axis and **o** defines the zero rotation angle and is coplanar with **n** and **h**. (b) Mapping of points in rotation space around the helix to a 40° PISA wheel.

NIH-PA Author Manuscript

NIH-PA Author Manuscript

NIH-PA Author Manuscript

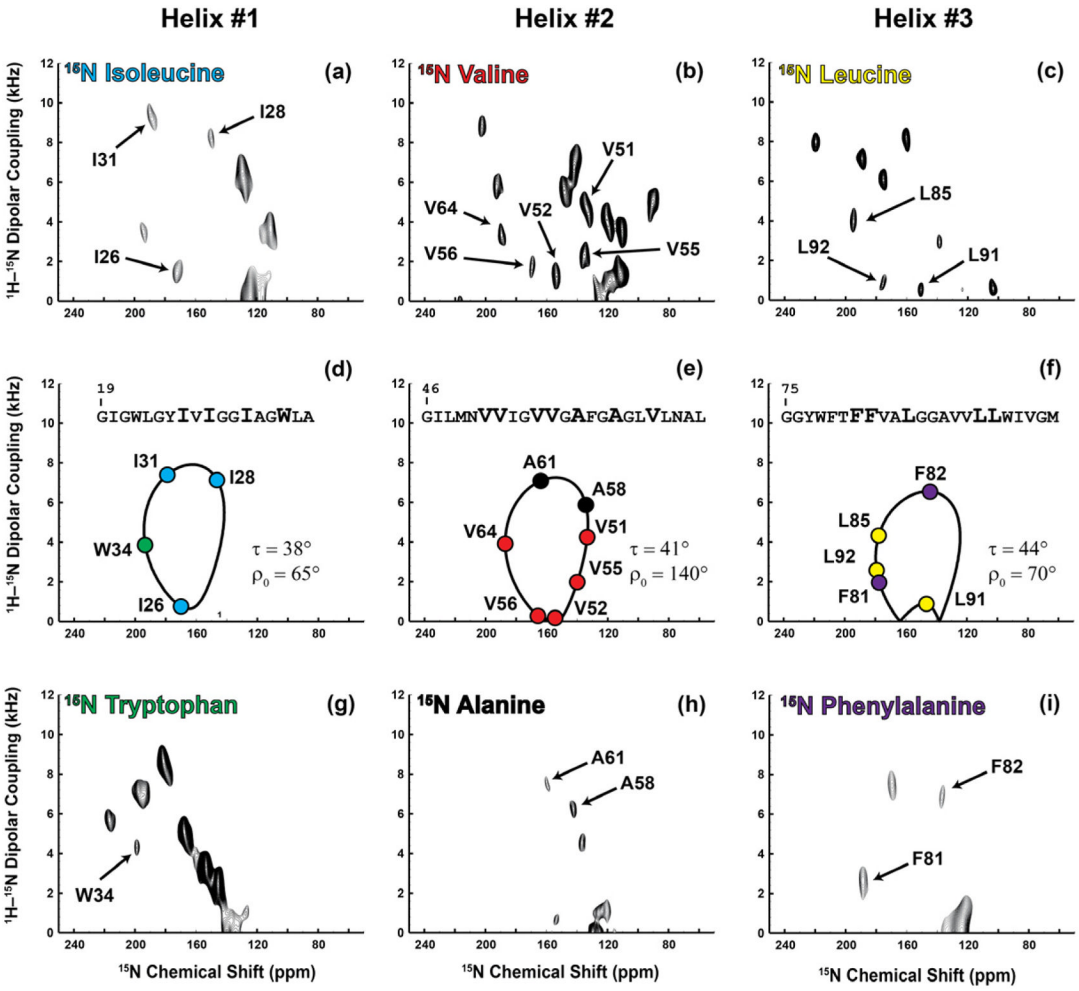

Fig. 4.

Assignment of core helical residues. AA specific ^{15}N-labeled spectrum, (a), (b), (c), (g), (h) and (i), used to assign the core residues (bold font in the sequences) of the three helices of Rv1861. Labeled amino acid type is indicated on each panel and color coded. (d), (e) and (f) theoretical PISA wheel patterns for each helix with predicted resonances color coded by amino acid type. Assignments were made by changing the tilt and rotation angles until a best-fit of the predicted frequencies to the experimental data was achieved. Helix one was assigned using panels (a) and (g), helix two was assigned using panels (b) and (h) and helix three was assigned using panels (c) and (i). The predicted helical sequences are displayed in panels (d), (e) and (f). 30–50 contours are plotted starting between 4σ and 9σ, increasing by a factor of 1.05 for the spectra in (a), (b), (c), (g), (h) and (i).

NIH-PA Author Manuscript

NIH-PA Author Manuscript

NIH-PA Author Manuscript

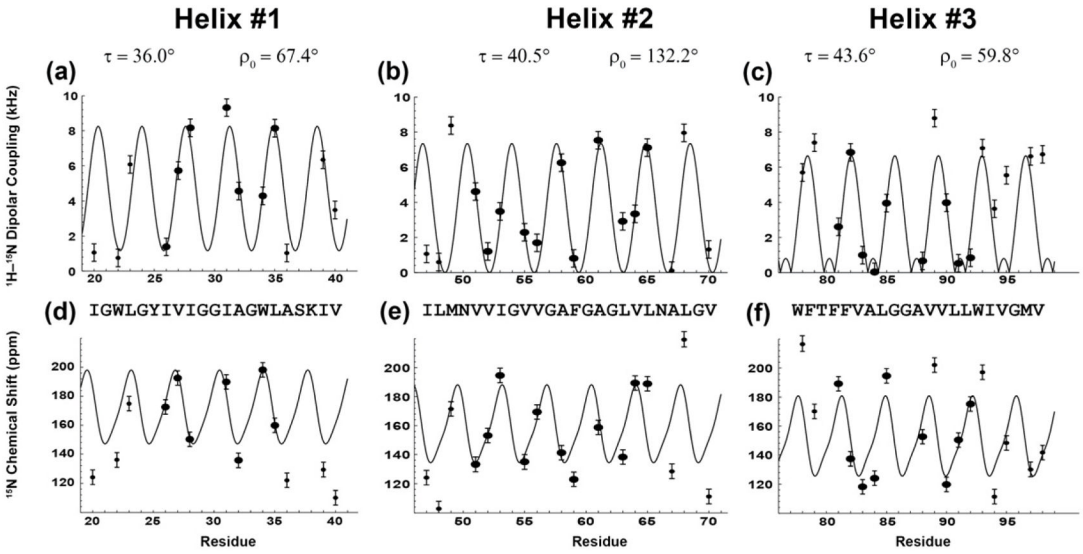

Fig. 5.

Wave Analysis. Dipolar, (a), (b), and (c), and anisotropic ^{15}N chemical shift, (d), (e), and (f), wave plots for each helix of Rv1861. Theoretical patterns are depicted by solid lines. Core residue assignments used in the best-fit minimization procedure are indicated by large circles. Assignments made after the core residues were assigned are indicated by small circles. The assignments are consistent with tilt/rotation angles as indicated. Error bars represent ±0.5 kHz in the dipolar plot and ±5 ppm in the chemical shift dimension.

NIH-PA Author Manuscript

NIH-PA Author Manuscript

NIH-PA Author Manuscript

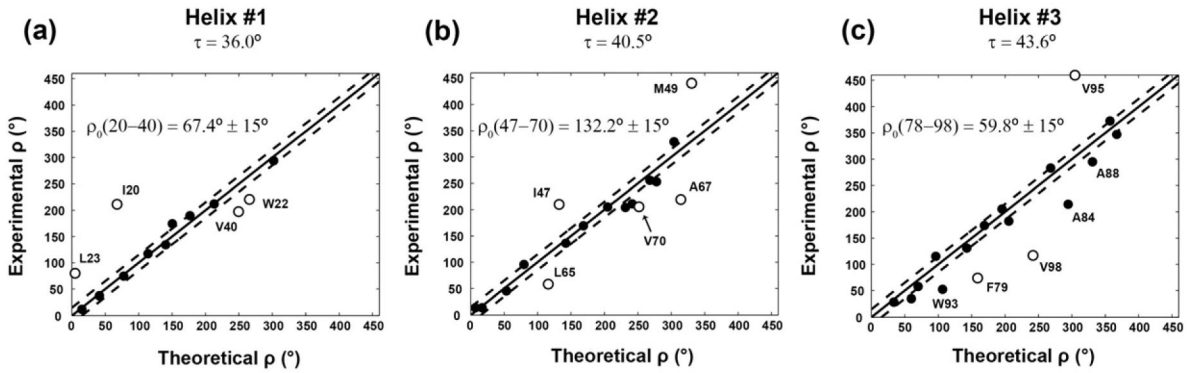

Fig. 6.

Δρ Analysis. (a) – (c) Δρ plots of the difference between experimental and predicted rotation angles for each assigned site. Dashed lines indicate ±15° deviations from an ideal helix. Labeled sites indicate deviations greater than 30°. Residues at the termini of a helix are represented by open circles and all others by solid circles.

NIH-PA Author Manuscript

NIH-PA Author Manuscript

NIH-PA Author Manuscript

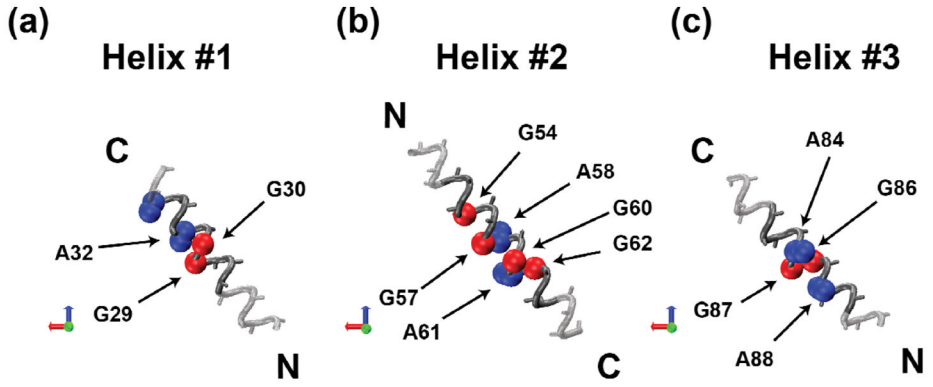

Fig. 7.

Glycine-Alanine Packing Surfaces. (a) – (c) Model helices based on the experimentally determined tilt and rotation angles for each helix of Rv1861. Glycine C_α residues are shown as red spheres, alanine C_α/C_β residues as blue spheres and all other residues represented as C_α/C_β bonds. Translucent sections of helix reside outside the well-defined core region for each helix.

NIH-PA Author Manuscript
NIH-PA Author Manuscript
NIH-PA Author Manuscript

Table 1

Predicted Amino acid content of the TM helices of Rv1861

Amino acid content by helix as predicted by the TMHMMv2.0 program [41].

Residue	Helix 1	Helix 2	Helix 3	All TM	Total
Glycine	5	5	5	15	23
Valine	1	5	4	10	14
Leucine	2	4	3	9	10
Isoleucine	4	2	1	7	9
Alanine	2	3	2	7	9
Phenylalaine	-	1	3	4	5
Tryptophan	2	-	2	4	4
Tyrosine	1	-	1	2	2
Methionine	-	1	1	2	5
Asparagine	-	2	-	2	4
Serine	1	1	-	2	3
Threonine	-	-	1	1	1
Total	18	24	23	65	89/101

NIH-PA Author Manuscript

NIH-PA Author Manuscript

NIH-PA Author Manuscript

Table 2
Assigned chemical shifts and dipolar couplings

Observed chemical shift and dipolar couplings for the TM helices of Rv1861. Residues from the core region of each TM domain used in the minimization procedure are in bold font.

Residue	^{15}N Chemical Shift (ppm)	^{1}H-^{15}N Dipolar Coupling (kHz)
Helix 1		
I20	124.2	1.055
W22	136.0	0.750
L23	174.9	6.078
I26	**172.6**	**1.384**
V27	**192.6**	**5.727**
I28	**150.2**	**8.165**
I31	**189.9**	**9.322**
A32	**135.7**	**4.564**
W34	**198.2**	**4.291**
L35	**159.9**	**8.144**
A36	122.1	1.126
I39	129.4	6.346
V40	110.1	3.489
Helix 2		
I47	124.2	1.055
L48	102.9	0.588
M49	171.5	8.371
V51	**133.2**	**4.615**
V52	**153.1**	**1.195**
I53	**194.6**	**3.485**
V55	**134.9**	**2.290**
V56	**169.4**	**1.689**
A58	**141.2**	**6.250**
F59	**123.0**	**0.800**
A61	**158.7**	**7.533**
L63	**138.2**	**2.916**
V64	**189.4**	**3.342**
L65	**188.9**	**7.112**
A67	128.5	0.100
L68	219.3	7.952
V70	111.2	1.307
Helix 3		
W78	216.5	5.695
F79	170.1	7.395
F81	**189.2**	**2.605**
F82	**137.3**	**6.841**
V83	**118.2**	**0.986**

NIH-PA Author Manuscript

NIH-PA Author Manuscript

NIH-PA Author Manuscript

Residue	^{15}N Chemical Shift (ppm)	^{1}H-^{15}N Dipolar Coupling (kHz)
A84	**124.1**	**0.030**
L85	**194.6**	**3.952**
A88	**152.6**	**0.655**
V89	202.1	8.794
V90	**119.8**	**3.979**
L91	**150.3**	**0.520**
L92	**175.2**	**0.835**
W93	197.1	7.080
I94	111.4	3.630
V95	148.2	5.539
M97	130.1	6.614
V98	141.6	6.732

NIH-PA Author Manuscript

NIH-PA Author Manuscript

NIH-PA Author Manuscript

Table 3

Best-Fit Tilt and Rotation Angles

Best-fit orientation angles for each TM helix of Rv1861. Final tilt and rotation angles are derived from minimization procedure of deviations between experimental and theoretical resonance positions for the core region residues of each helix.

Helix	Initial Tilt (°)	Final Tilt (°)	Initial Rotation[a] (°)	Final Rotation[a] (°)
1	38.0	36.0	65.0	67.4
2	41.0	40.5	140.0	132.2
3	44.0	43.6	70.0	59.8

[a]Rotation angles are defined from I20, I47 and W78 for helices one, two and three, respectively.